Electronic Supplementary Information

Imidazole assisted film-based fluorescent sensor for ultrasensitive detection of hydrazine

*Mohammad Masood Zafar,[a] Subash Ch. Sahoo,[b] Vakayil K. Praveen,[c,d] Nidhi Tyagi,[*e] and Rakesh K. Mishra[*a]*

[a.]Department of Chemistry, National Institute of Technology Uttarakhand (NITUK), Srinagar (Garhwal)-246174, Uttarakhand, India; [b.]Department of Chemistry, Panjab University, Chandigarh–160014, India; [c]Chemical Sciences and Technology Division, CSIR-National Institute for Interdisciplinary Science and Technology (CSIR-NIIST), Thiruvananthapuram – 695019, Kerala, India; [d]Academy of Scientific and Innovative Research (AcSIR), Ghaziabad 201002, India; [e.]School of Chemical Sciences, Amity University Punjab, Sector 82A, IT City, International Airport Road, Mohali–140306, Punjab, India.

TABLE OF CONTENTS

1. FT-IR, ¹H NMR, ¹³C NMR, and HRMS spectra of the compounds 1, R-1 and R-2
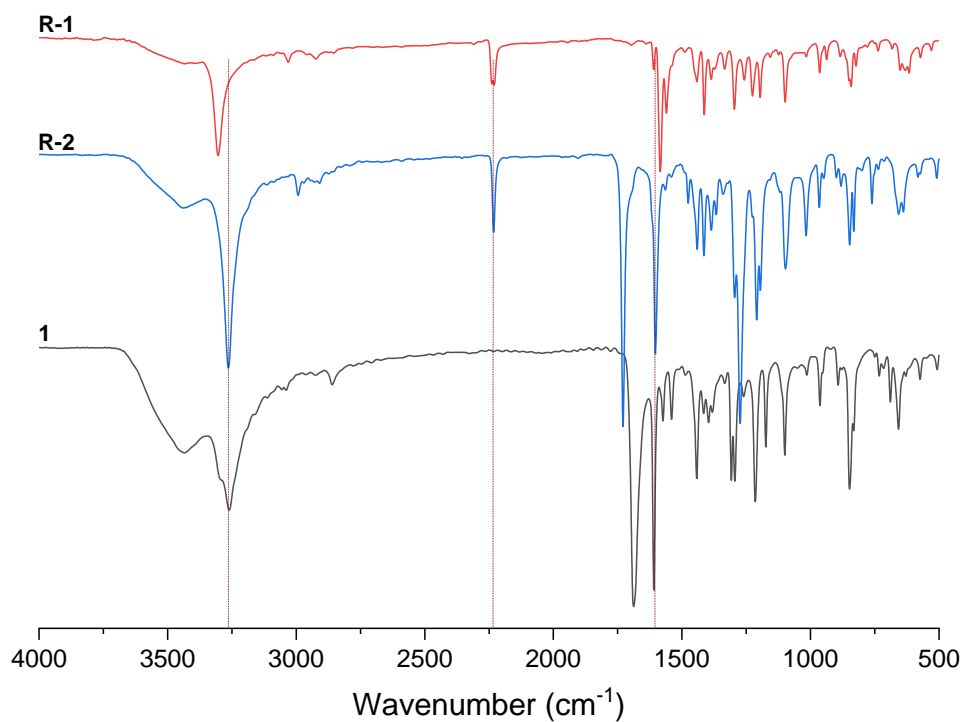
Fig. S1 Overlay FT-IR spectra of the compounds **1**, **R-1** and **R-2**.
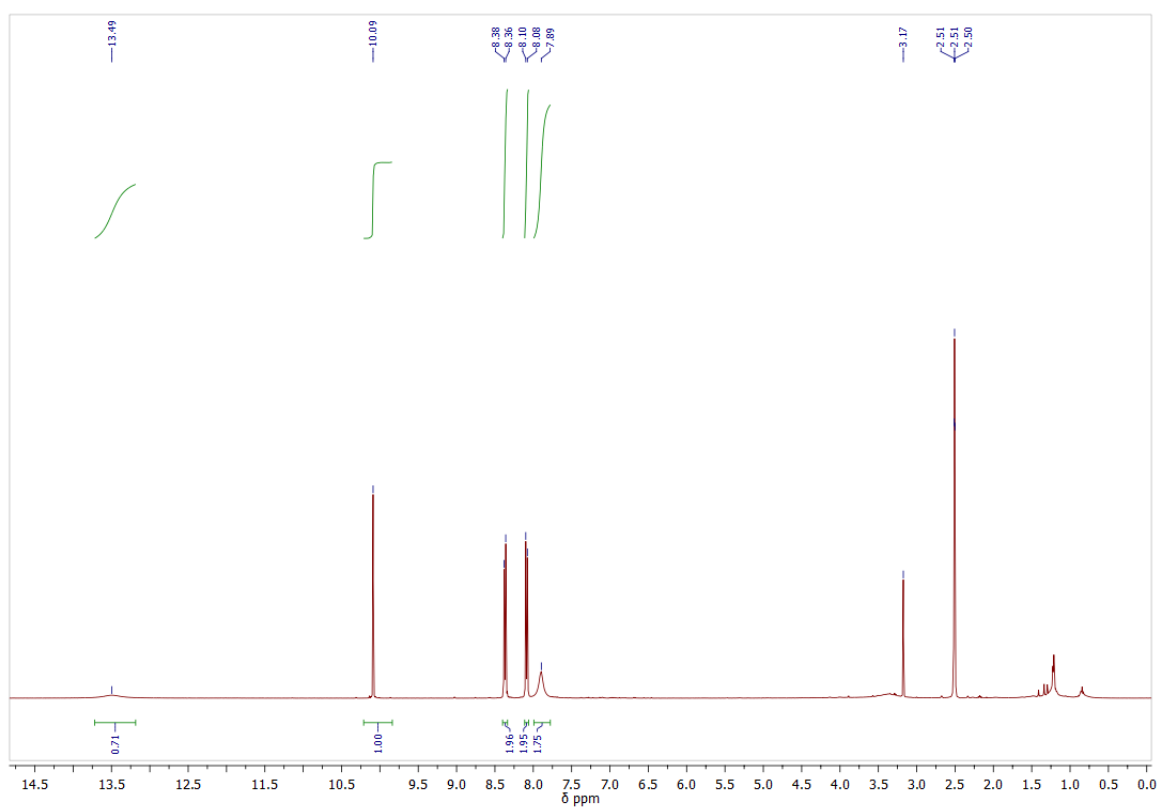
Fig. S2 ¹H NMR (500 MHz) spectrum of **1** in DMSO-d_6.

Fig. S3 ^{13}C NMR (125 MHz) spectrum of compound **1** in DMSO-d_6.

Fig. S4 HRMS spectrum of compound **1**.

Fig. S5 ^{1}H NMR (500 MHz) spectrum of compound **R-1** in DMSO-d_6.

Fig. S6 ^{13}C NMR (125 MHz) spectrum of compound **R-1** in DMSO-d_6.

Fig. S7 HRMS spectrum of compound **R-1**.

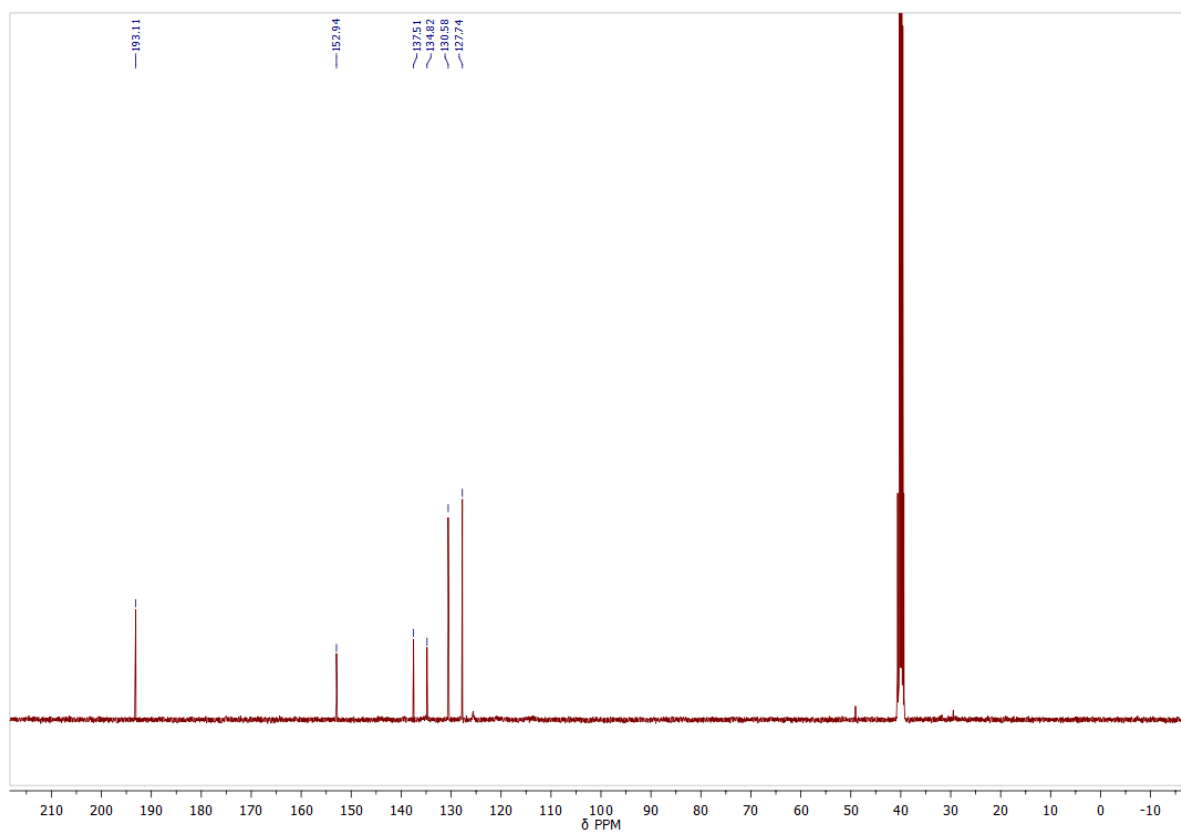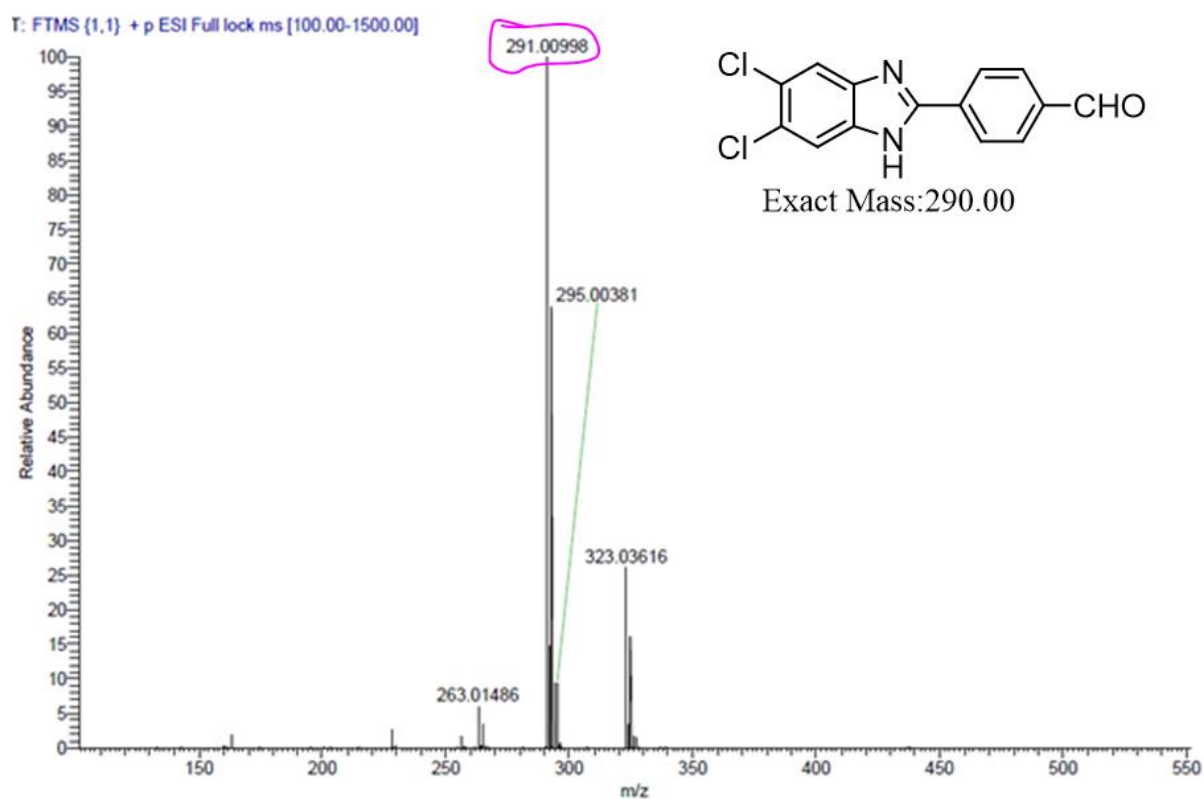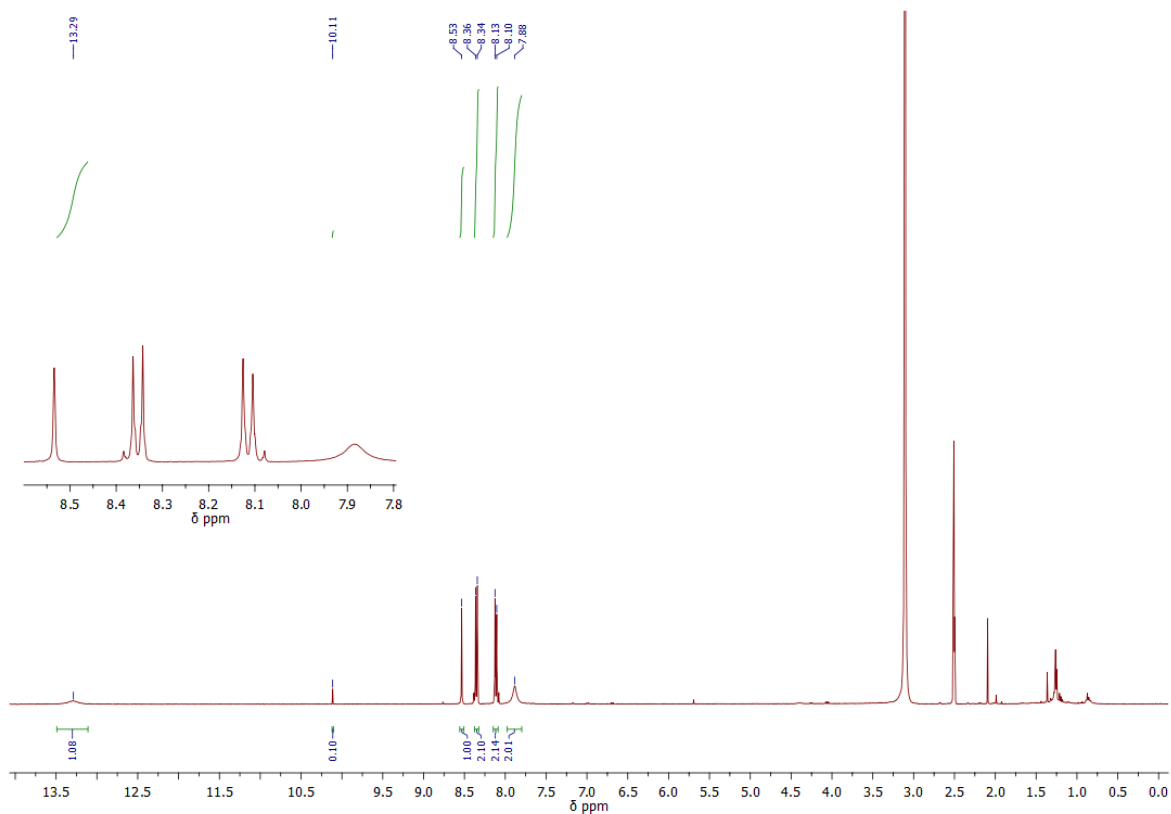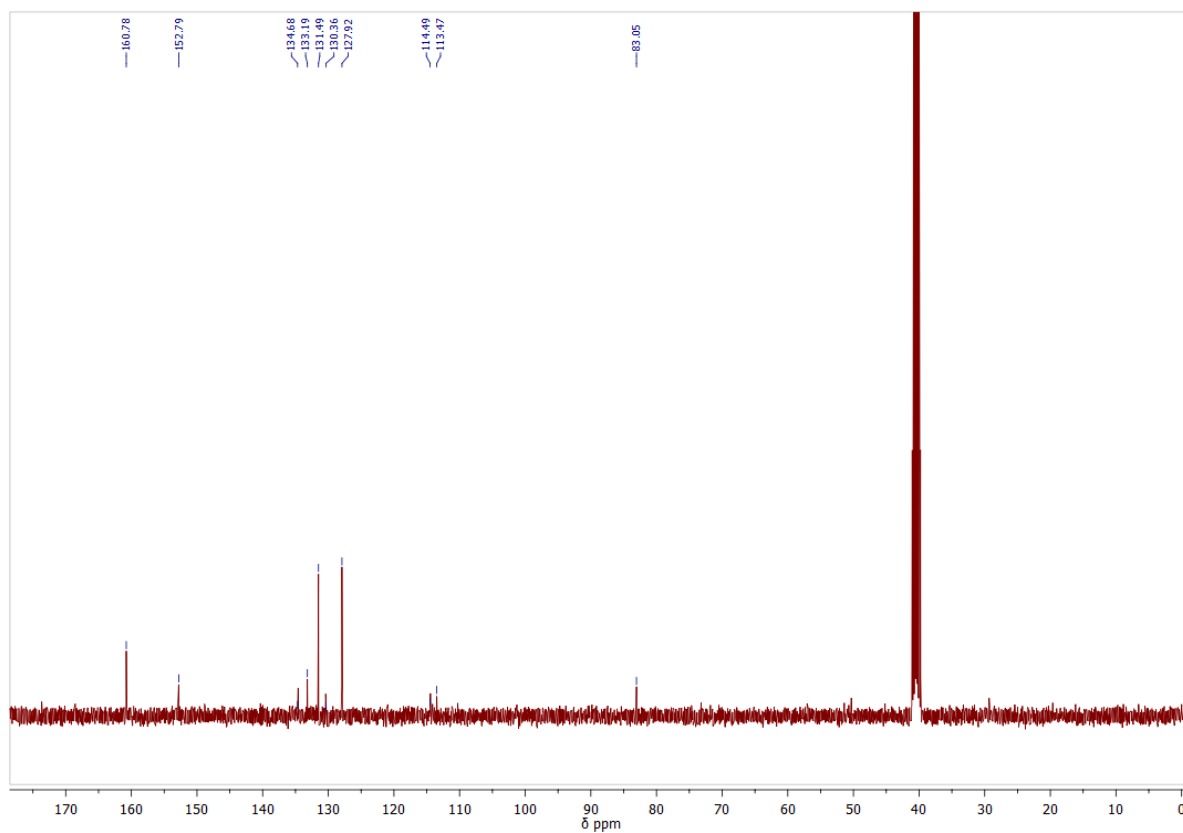**Fig. S8** ^{1}H NMR (500 MHz) spectrum of compound **R-2** in DMSO-d_6.

Fig. S9 ^{13}C NMR (125 MHz) spectrum of compound **R-2** in DMSO-d_6.

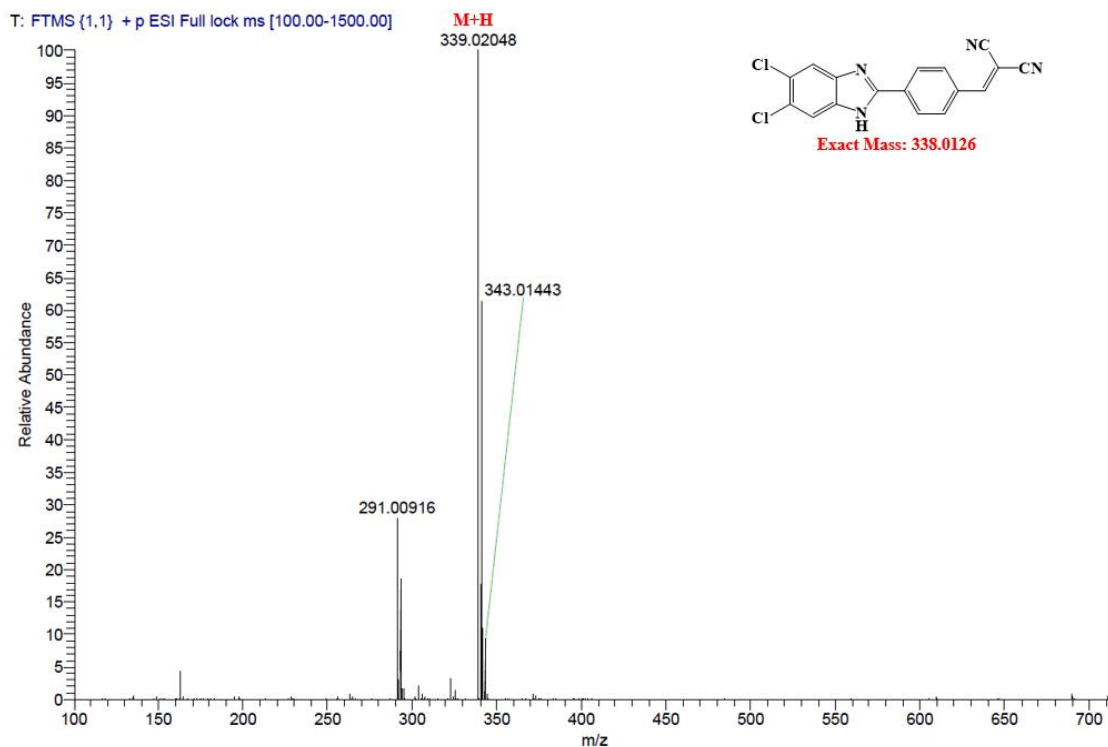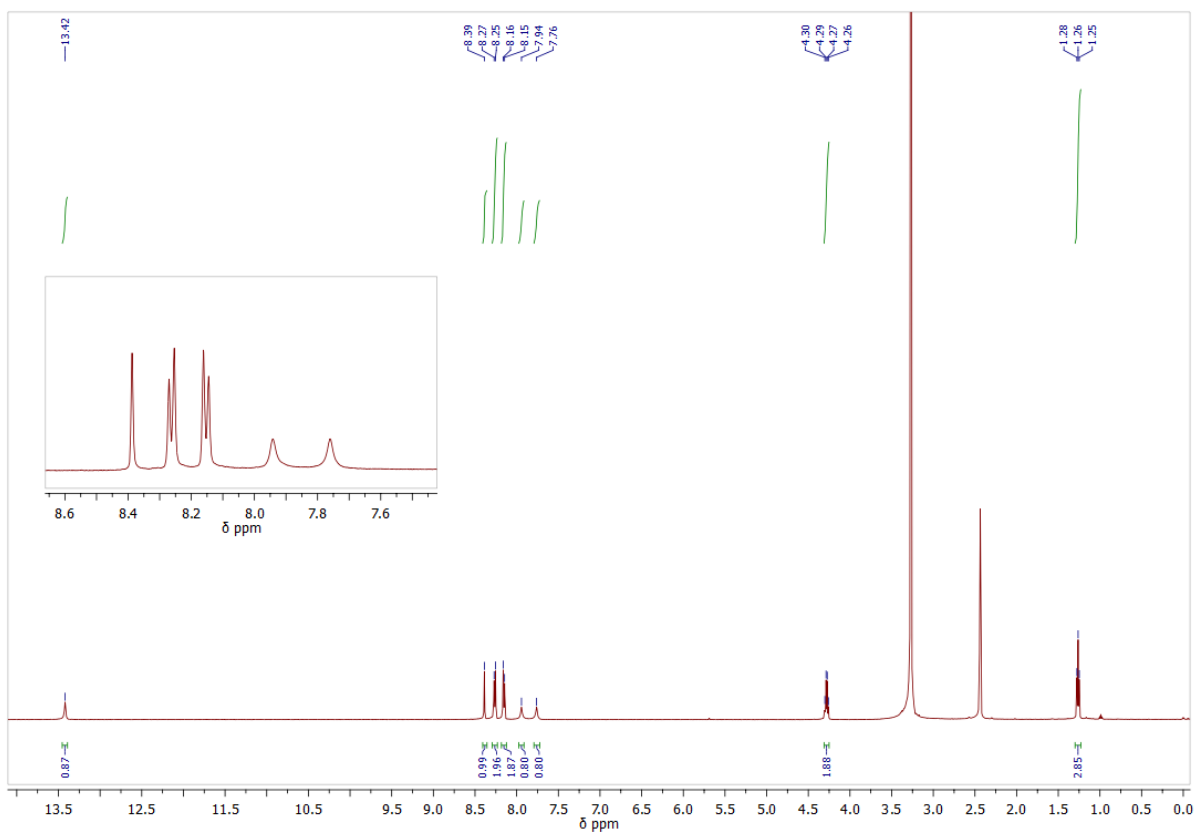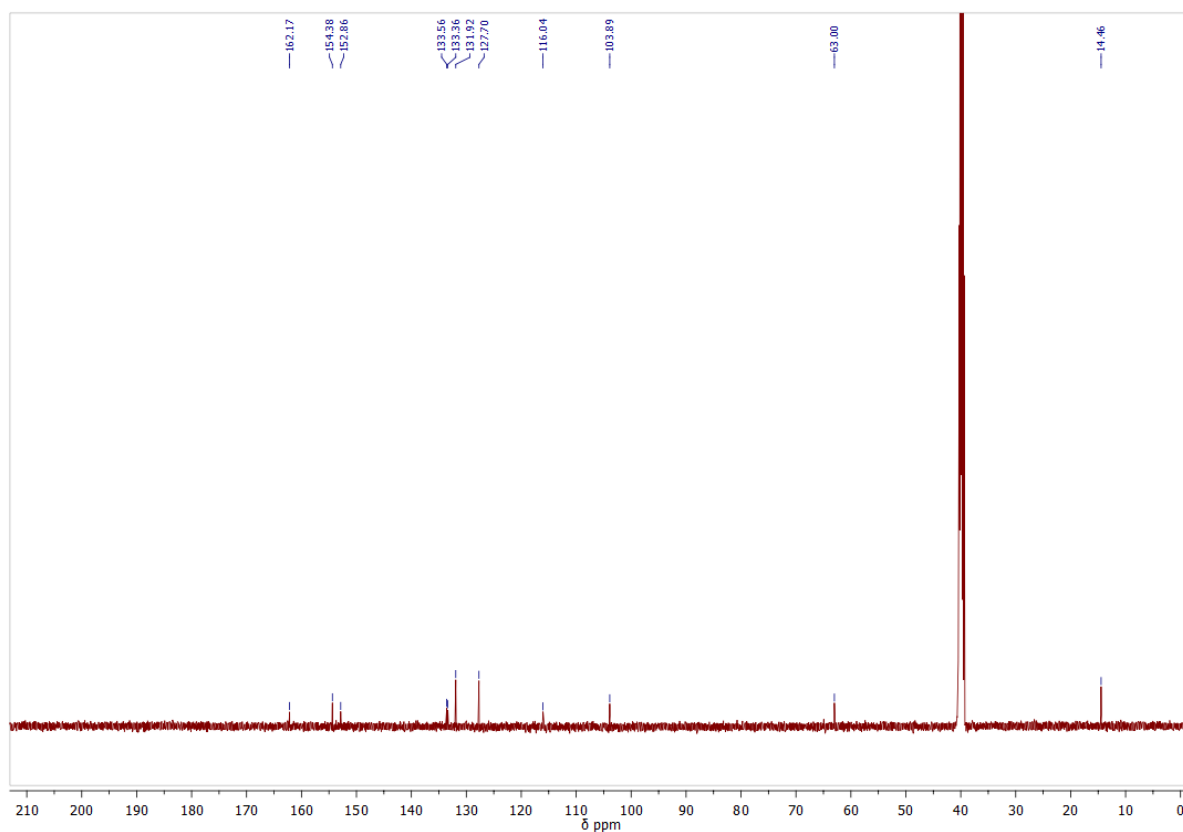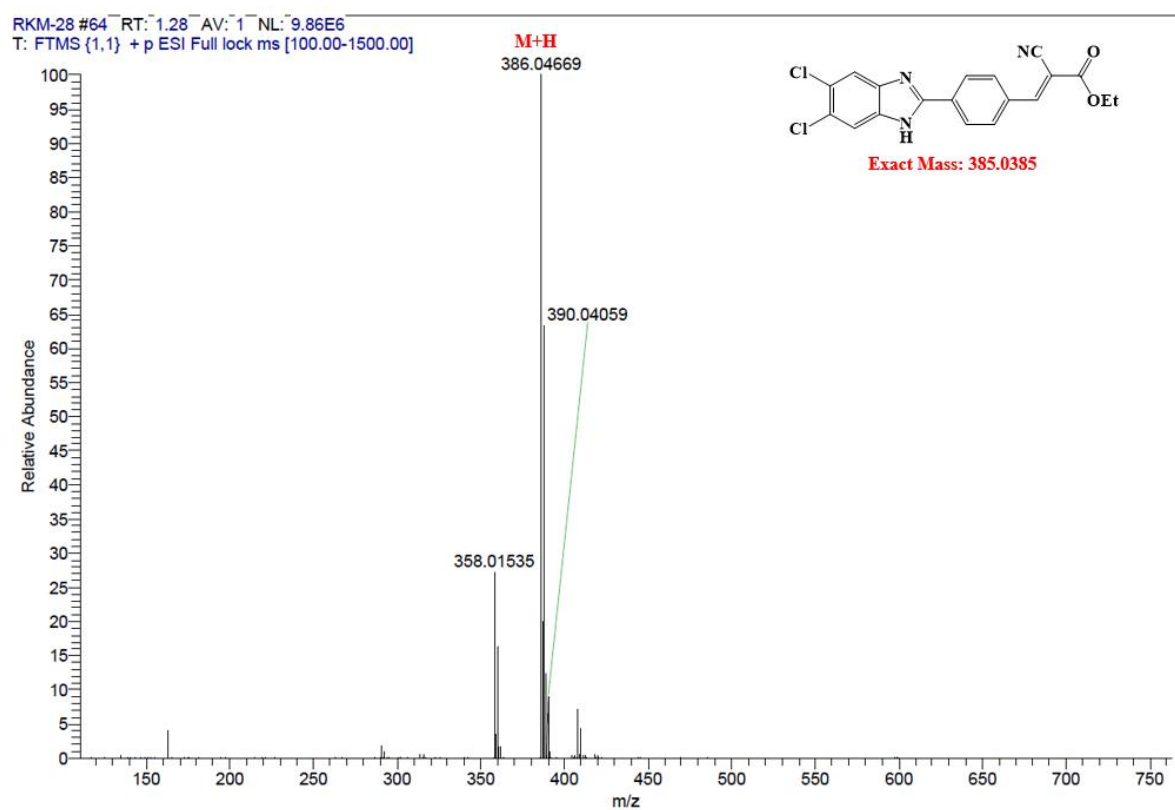**Fig. S10** HRMS spectrum of compound **R-2**.

2. Crystallographic data

2.1. Table S1. Selected crystallographic data of R-1 and R-2.

Data	R-1	R-2
Chemical formula	$C_{17}H_8Cl_2N_4 \cdot C_3H_7NO$	$2(C_{19}H_{13}Cl_2N_3O_2)$
Formula Mass	412.27	772.45
Crystal system	Triclinic	Triclinic
a/Å	7.8572(2)	9.7546(3)
b/Å	10.5742(4)	13.6517(4)
c/Å	12.2644(3)	15.5974(5)
α/°	104.009(2)	65.830(3)
β/°	92.066(2)	89.235(2)
γ/°	102.979(3)	70.210(2)
Unit cell volume/Å^3	958.99(5)	1763.97(10)
Temperature/K	293(2)	293(2)
Space group	$P\bar{1}$	$P\bar{1}$
No. of formula units per unit cell, Z	2	2
Radiation type	MoKα	MoKα
Absorption coefficient, μ/mm^{-1}	0.360	0.387
No. of reflections measured	12370	24165
No. of independent reflections	3904	7447
R_{int}	0.0476	0.0470
Final R_1 values ($I > 2\sigma(I)$)	0.0493	0.0502
Final $wR(F^2)$ values ($I > 2\sigma(I)$)	0.1161	0.1154
Final R_1 values (all data)	0.0723	0.0898
Final $wR(F^2)$ values (all data)	0.1329	0.1329
Goodness of fit on F^2	1.049	1.037
CCDC No	**2309138**	**2309139**

2.2. Table S2. Selected parameters for weak interactions in R-1 and R-2.
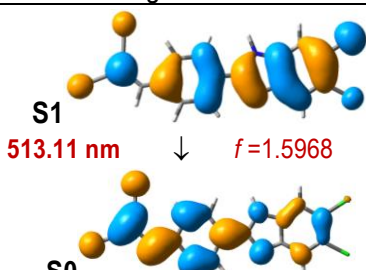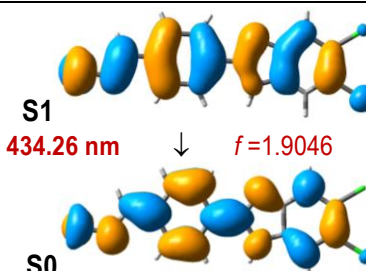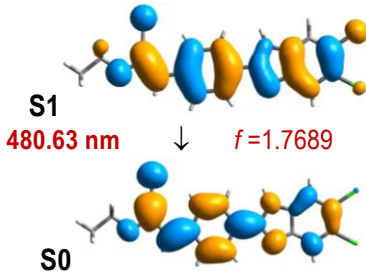
R-1			R-2		
Short Contact	Bond length (Å)	Symmetry Code	Short Contact	Bond length (Å)	Symmetry Code
$N_1 \cdots O_1$	2.863	x, y, z	$N_2 \cdots N_{24}$	2.906	2-x, -y,1-z
$C_{17} \cdots O_1$	3.136	x,1+y, z	$H_2 \cdots N_{24}$	2.080	2-x, -y,1-z
$Cl_1 \cdots C_{18}$	3.377	1-x, -y,1-z	$O_{22} \cdots H_{14}$	2.611	2-x,1-y,1-z
$Cl_2 \cdots Cl_2$	3.386	1-x, -y, -z	$O_{22} \cdots H_{38}$	2.548	x, y, z
$H_1 \cdots O_1$	2.028	x, y, z	$C_1 \cdots H_{46B}$	2.877	2-x,1-y,1-z
$H_1 \cdots C_{18}$	2.598	x, y, z	$Cl_{51} \cdots H_{47A}$	2.852	-1+x, -1+y,1+z
$H_{13} \cdots O_1$	2.580	x, y, z	$Cl_{52} \cdots Cl_{52}$	3.283	-x,1-y, 2-z
$N_2 \cdots H_{18}$	2.465	1-x,1-y,1-z	$C_{33} \cdots H_{38}$	2.842	1-x,1-y,1-z
			$N_{28} \cdots N_{50}$	2.952	1-x,2-y,1-z
			$N_{50} \cdots H_{28}$	2.079	1-x,2-y,1-z

3. Theoretical Data

3.1. Table S3: Comparison of absorption properties of **R-1**, **R-1-**N_2H_4 and **R-2** with the simulated excitation energy, oscillator strength and percentage contributions of the orbital for different transitions.

Compound	Experimental	Theoretical				
	λ_{max} (nm)	λ(nm)	f	Orbitals & Contribution (%)		
R-1	380	421.00	0.9096	HOMO	→ LUMO	99.14
		387.46	0.0041	HOMO-1	→ LUMO	99.19
		310.96	0.4718	HOMO-3	→ LUMO	12.07
				HOMO-2	→ LUMO	76.84
				HOMO	→ LUMO+1	09.85
R-1+N_2H_4	345	340.30	1.3091	HOMO	→ LUMO	97.53
		298.95	0.0162	HOMO-1	→ LUMO	93.29
		287.73	0.0202	HOMO-2	→ LUMO	79.62
				HOMO	→ LUMO+1	16.85
R-2	370	371.28	1.2061	HOMO	→ LUMO	98.47
		326.09	0.0065	HOMO-1	→ LUMO	97.55
		303.76	0.2233	HOMO-2	→ LUMO	81.03
				HOMO	→ LUMO+1	16.16

3.2. Table S4: Comparison of emission properties of **R-1**, **R-1**-N_2H_4 and **R-2** with the simulated emission wavelength, oscillator strength and orbital involved.

Compound	Emission Wavelength, λ_{em} (nm)			
	Experimental			Theoretical
	DMSO	Solid State	**R-1**$_{Gel}$	Oscillator Strength and Orbitals involved
R-1	560	550	540	 **S1** **513.11 nm** ↓ *f* =1.5968 **S0**
R-1+N_2H_4	405 & 428	438*	468	 **S1** **434.26 nm** ↓ *f* =1.9046 **S0**
R-2	540	485 & 510	-	 **S1** **480.63 nm** ↓ *f* =1.7689 **S0**

*In case of **R-2** the intensity at 485 & 510 is reduced as it took longer time to complete the reaction.

4. Aggregation studies of compounds R-1 and R-2

The fluorescence properties of **R-1** and **R-2** have been investigated in DMSO/water solvent mixtures in order to evaluate their Aggregation Induced Emission (AIE) properties. As shown in Figure S11, **R-1** is strongly emissive in pure DMSO, while increasing the water content in DMSO/water mixtures from 0 to 90%, the fluorescence intensity was first increased (up to 30% water content) and was reduced and blue shifted there after (up to 90% composition of water). Similarly the **R-2** was found to be strongly emissive in the 80% water/DMSO mixture.
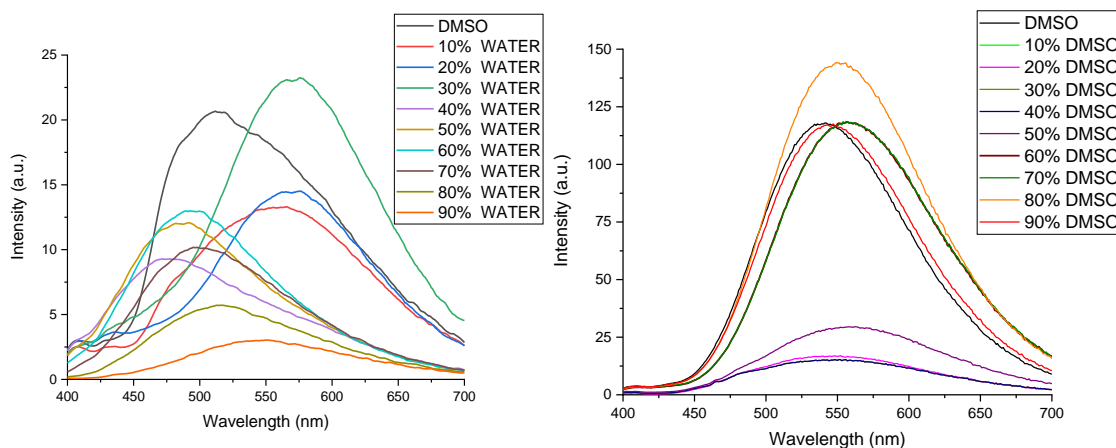

Fig. S11 Fluorescence spectra of a) **R-1** and b) **R-2** in DMSO-Water mixtures with different water fractions (λ_{ex} = 370 nm).

4.1. Viscosity experiments and lifetime studies

The **R-1** and **R-2** both planer molecule and represents the D–π–A type rotor through the π-conjugated linker. The rotatable parts, including the benzene rings and linker of π-bridge (carbon–carbon double bond), can rotate freely in low-viscous media, resulting in a non-radiative quenching of the excited state and consequently are less or non-emissive. While, in high-viscous media, intramolecular motions are inhibited, and energy is released through radiative decay, resulting in stronger fluorescence.

Considering this, the viscosity-responsive optical performance was investigated in more detail with a methanol–glycerol system with various glycerol fractions (f_G = 0-90, vol%). As **R-2** showed better AIE properties, in order to explore the mechanism, fluorescence change of probe **R-2** for was monitored at different glycerol-MeOH fractions (f_G = 0-90, vol%). It was observed that on increasing the glycerine content (0 → 90, vol%), the emission intensity at 540 nm has increased (**Fig. S12a**). The signal was rather weak up to f_G = 60%, while the intensity increased sharply with a higher f_G exceeding 60%, and it reached nearly 2-fold in the mixed solution with f_G = 90%. The enhancement in emission has also been supported by the lifetime measurement data of **R-2** (τ_{av} = 5.44 ns, f_G = 0; τ_{av} = 21.47ns, f_G = 90) and **R-1** (τ_{av} = 12.32 ns, f_G = 0; τ_{av} = 16.78 ns, f_G = 90) in viscous medium which showed the enhanced life time due to aggregation (**Fig. S12c** and **12d**).
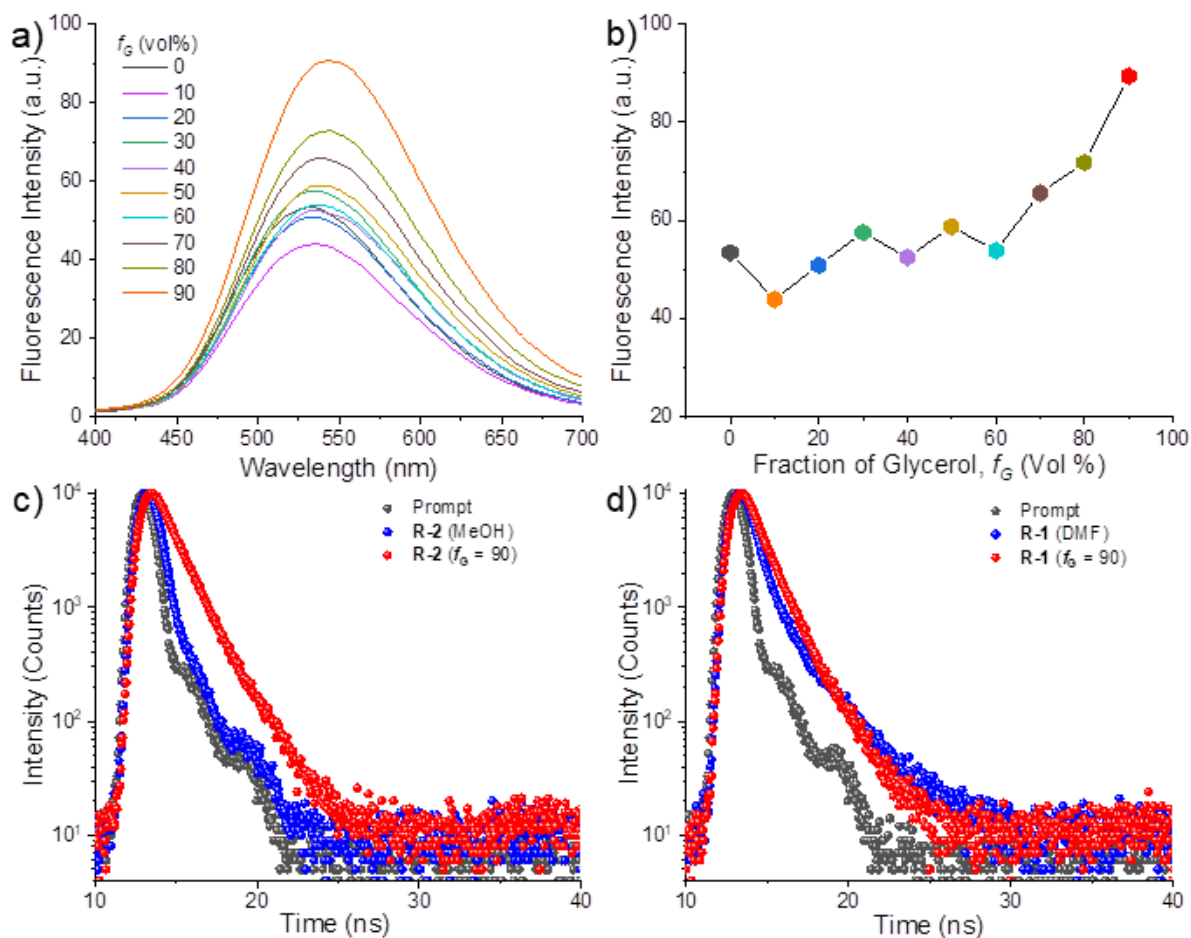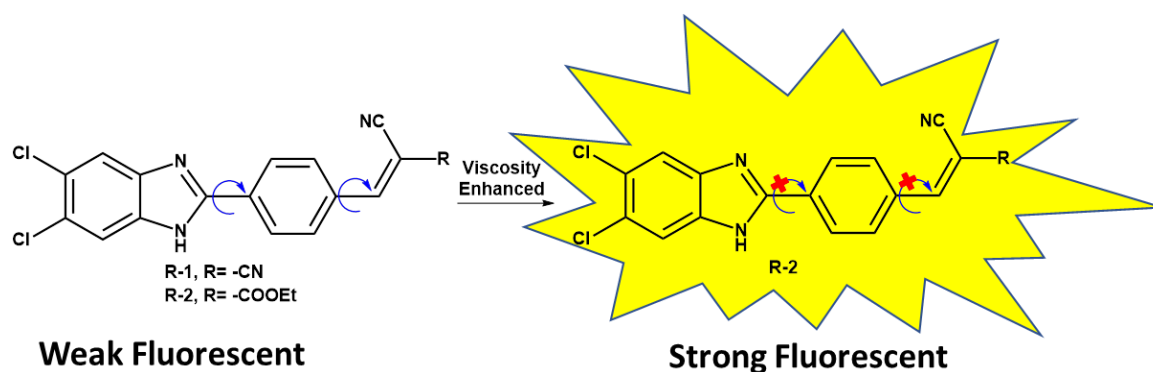
Fig. S12 a) Fluorescence (λ_{ex} = 370 nm) spectra of **R-2** (30 μM) with different glycerol fraction (f_G = 0-90, vol%), b) Change in intensity at 540 nm with respect to different glycerol fraction (f_G = 0-90, vol%), c) Lifetime (λ_{ex} = 370 nm) recorded for **R-2** in MeOH and 90% glycerol-MeOH (f_G = 90) **R-2** and d) lifetime (λ_{ex} = 370 nm) recorded for **R-1** in DMF and 90% glycerol-DMF (f_G = 90) medium.

4.1. Scheme showing the mechanism of the enhanced emission of R-1 and R-2

Thus the above experiments support that enhanced emission is observed due to the restricted intermolecular rotation (RIR) in both **R-1** and **R-2** (**Scheme S1**)

Scheme S1. Mechanism of the enhanced emission of **R-1** and **R-2.**
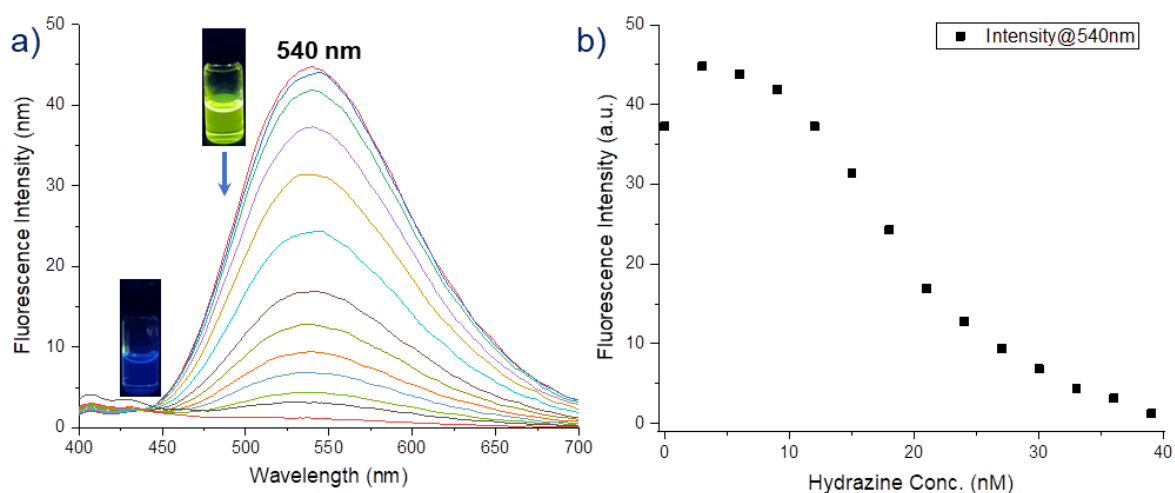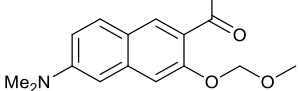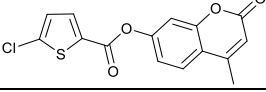
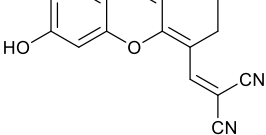## 5. Fluorescence Titration Studies of R-2
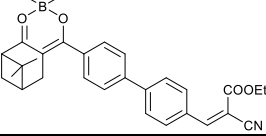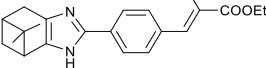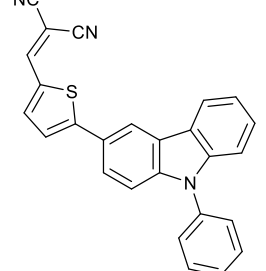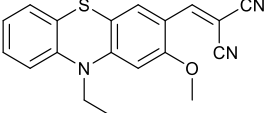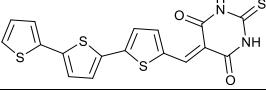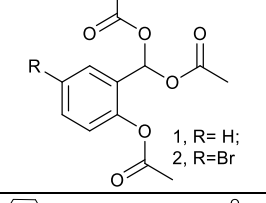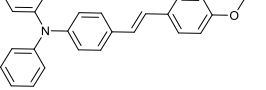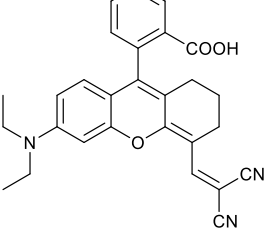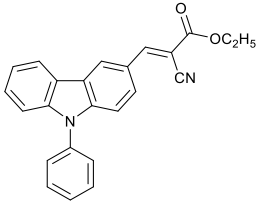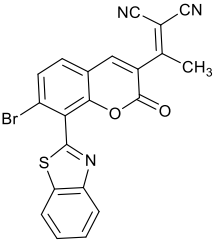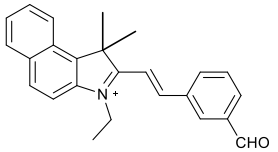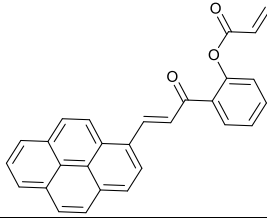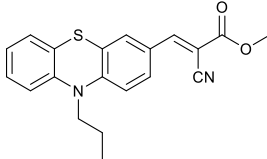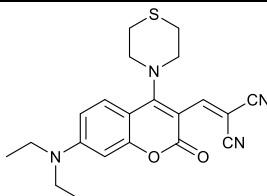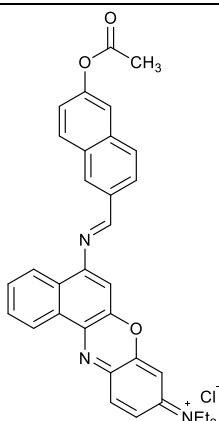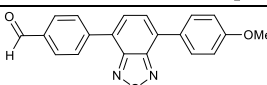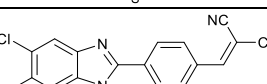
Fig. S13 a) Fluorescence (λ_{ex} = 370 nm) spectra of **R-2** (30 µM, DMSO) with increasing concentration of N_2H_4 (0.0 to 40 nM), b) Change in intensity at 540 nm with after addition of N_2H_4 (0.0 to 40 nM).

6. Table S5. Comparison data of previously reported N_2H_4 sensors with current data

S. No.	Probe Structure	Wavelength (nm), λ		Detection Limit	Response Time	Application	Year	Reference No
		Excitation (Probe)	Emission (Probe+N_2H_4)					
1.		395	460	3.4 nM (0.11 ppb)	2–3 min	-	2013	1
2.		350	510 & 400	1.79×10^{-9} M	40 s	Test Strips, HeLa cells	2016	2
3.		430	500	22.5 nM (0.716 ppb)	2 h	Test Strips, RAW264.7 Cells	2017	3
4.		520	545	26 nM (0.83 ppb)	5 min	Paper Strips, & HepG2 Cells	2018	4
5.		327	456	1.9 nM (0.06 ppb)	1 & 8 min	Real Water Samples and TLC Plates	2018	5
6.		670	701	0.78 ppb	1 h	Mouse Liver Slices	2018	6

No.	Structure	Abs (nm)	Em (nm)	LOD	Time	Application	Year	Ref
7.		391	496	0.035 ppb	60 min	Paper Strip, Soil Analysis, Spray Application, Tissues Imaging	2019	7
8.		375	450	0.0047 µM (1.5 ppb)	3 h	Tap Water and River Water Samples	2020	8
9.		500	651	0.09 µM (2.87 ppb)	1 h	Tap Water and River Water Samples; LO2 Cells	2020	9
10.		300	495 & 580	96.3 nM	40 s	TLC Plates, HeLa Cells	2020	10
11.		380	470	7.9×10^{-8} M	20 min	Lake Water & Mung Beans	2020	11
12.		370	604 & 442	42.5 nM	30 min	TLC Plate & U937 Cells	2020	12
13.		365	530	2.6 µM	5 min	TLC Plates & MCF-7 Cells	2020	13
14.		360	448	1.45 nM (0.04 ppb)	10 s	Silica, Filter Paper, HeLa Cells	2020	14
15.		366	500 & 456	1: 8.4 ppb 2: 8.7 ppb	2 min	Distilled Water, Tap Water, River Water & MCF-7 Cells	2020	15
16.		350	460	8.47 nM	3 min	Ground Water, Tap Water, River Water & HeLa Cells	2020	16
17.		515	645 & 565	0.08 µM (2.56×10^{-3} µg mL^{-1})	35 min (max.)	Drinking Water & HepG2 Cells	2021	17

No.	Structure	λex (nm)	λem (nm)	LOD	Response Time	Application	Year	Ref.
18.		390	445 & 535	1.5×10^{-6} M	<100 s	Paper Strips, Mung Bean Sprouts, Water Samples RAW264.7 Cells and Zebrafish	2021	18
19.		390	446	1.7 nM	~1 min	Filter Paper Strips and MDA-MB 231 cells	2022	19
20.		500	586	7.8 nM	80 s	HeLa and HepG2 cells	2022	20
21.		420	576, 415 and 393	1.9 nM,	15 min	Tap water, River Water, and Soil Sample	2022	21
22.		354	475	6.7 ppb	60 min	HepG2 Cells	2022	22
23.		400/470	496 & 560	0.32 μM	90 min	TLC plate, Cotton Swab, Soil Sample, HeLa cells	2023	23
24.		590	725	4.5×10^{-10} M	0-40 s	TLC & Paper Strips, Water and Soil Samples, MDA-MB-231 cancer cells	2023	24
25.		340	375	340 nM (10 ppb)	10 min	lipid droplets, C. elegans and zebrafish	2023	25
26.		370	550	0.08 ppb	1-2 min	Polymer Film, C6 (glial) cells	2024	This Work

7. Sensitivity of R-1 towards hydrazine vapour

(0 Min)   **(15 Min)**
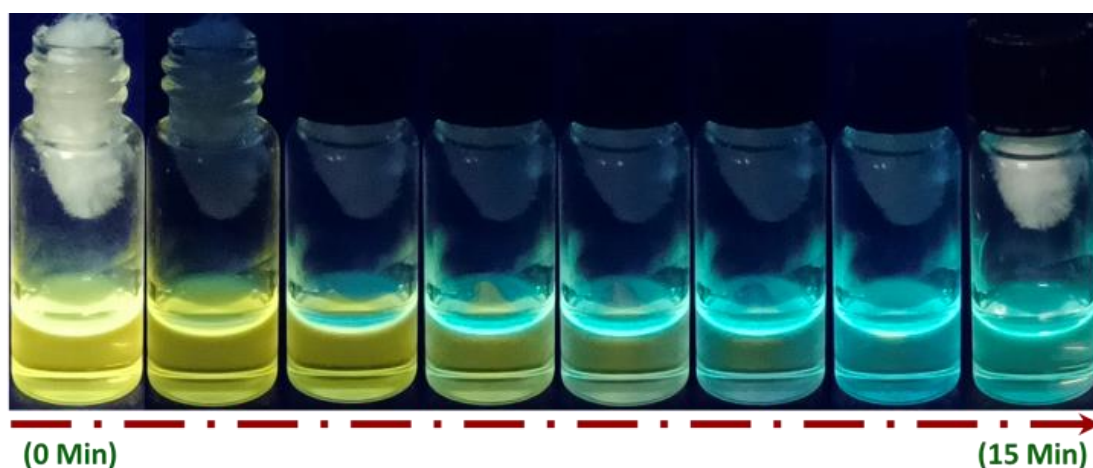
Fig. S14 Demonstration of the yellow fluorescence quenching (**R-1**) by hydrazine vapour.

8. HRMS spectrum of R-1–N$_2$H$_4$ product

305.03558 **(M+H)**
Chemical Formula: C$_{14}$H$_{11}$Cl$_2$N$_4$
Exact Mass: 305.0361

Chemical Formula: C$_{14}$H$_{10}$Cl$_2$N$_4$
Exact Mass: 304.0283
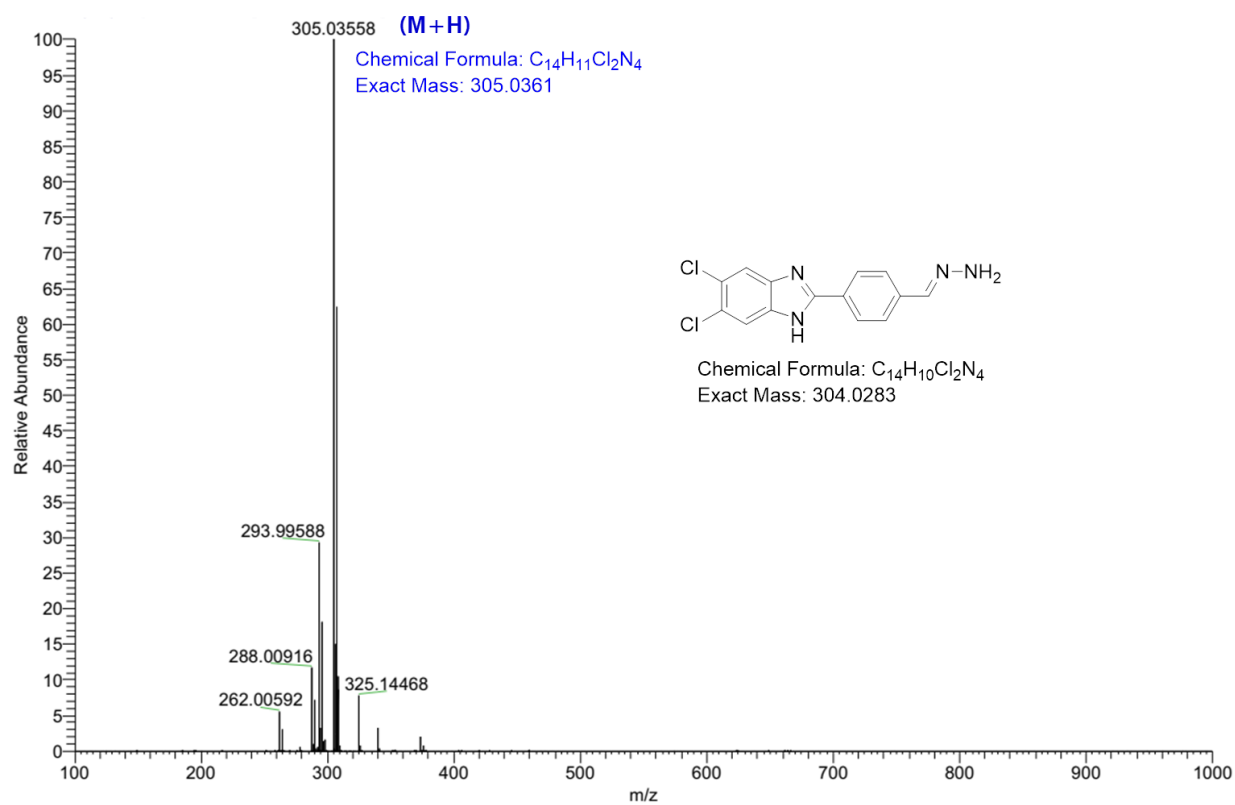
Fig. S15 HRMS spectrum of **R-1**-N$_2$H$_4$ adduct.

9. Optimized structure of R-1-N₂H₄ product and HOMO, LUMO
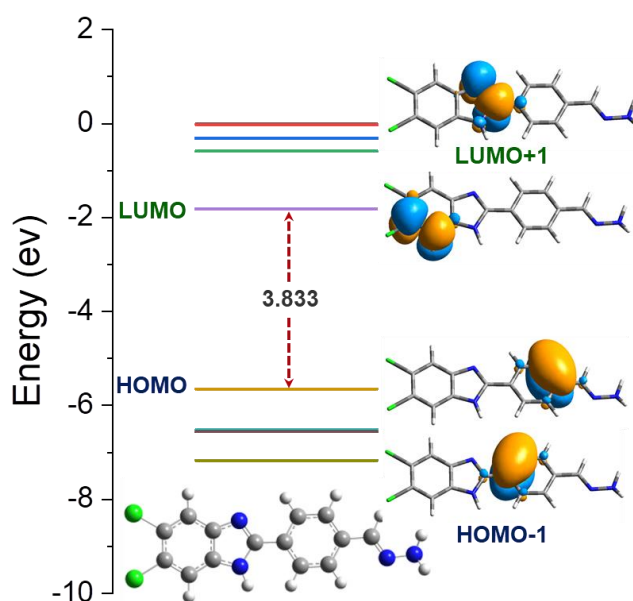
Fig. S16 The optimized structure of **R-1-N₂H₄**. The schematic representation of relative energy levels of the important orbitals as well as electronic distributions observed in frontier orbitals (HOMO, HOMO+1, LUMO and LUMO+1) of **R-1-N₂H₄** with band gap values using DFT/B3LYP/6-31G**.

10. Solid-state sensing studies of N₂H₄
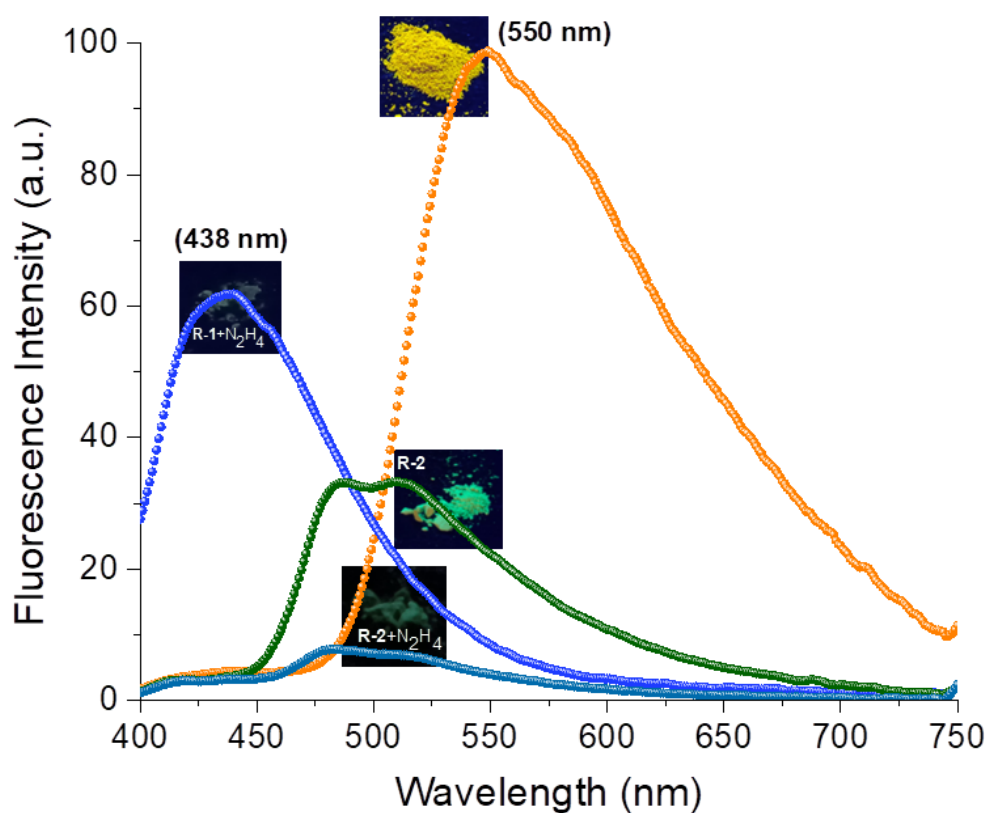
Fig. S17 Fluorescence spectra of **R-1** and **R-2** in solid state (λ_{ex} = 380 nm) and after addition of excess of hydrazine and the corresponding visual change in the fluorescence of **R-1** and **R-2**.

11. Temperature-dependant ^1H NMR studies of R-1

Fig. S18 Temperature Dependant ^1H NMR Studies of **R-1** in DMSO-d_6 at different temperature.

12. Cytotoxicity of R-1

Fig. S19 in vitro cytotoxicity in c6 cells treated with **R-1** at different concentrations.

13. Supplementary information references

1. Y. Tan, J. Yu, J. Gao, Y. Cui, Y. Yang and G. Qian, *Dye. Pigment.*, 2013, **99**, 966–971.

2. Shweta, A. Kumar, Neeraj, S. K. Asthana, A. Prakash, J. K. Roy, I. Tiwari, and K. K. Upadhyay, *RSC Adv.*, 2016, **6**, 94959–94966.

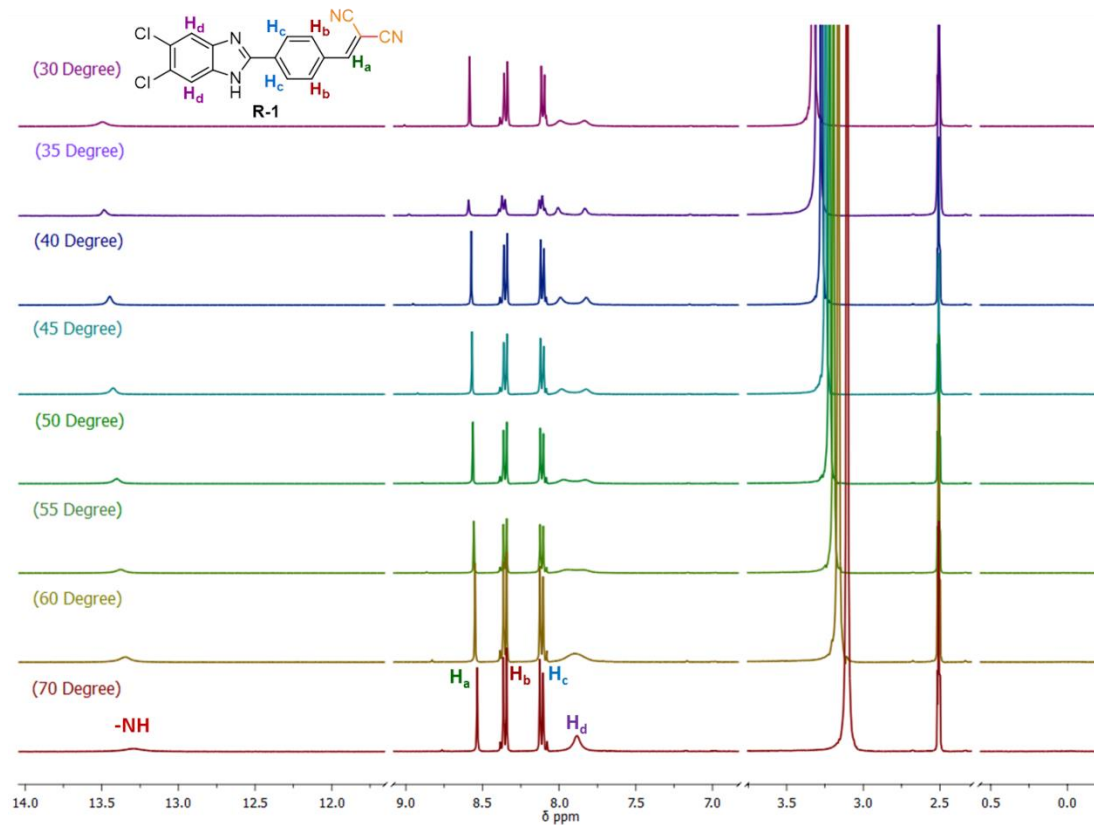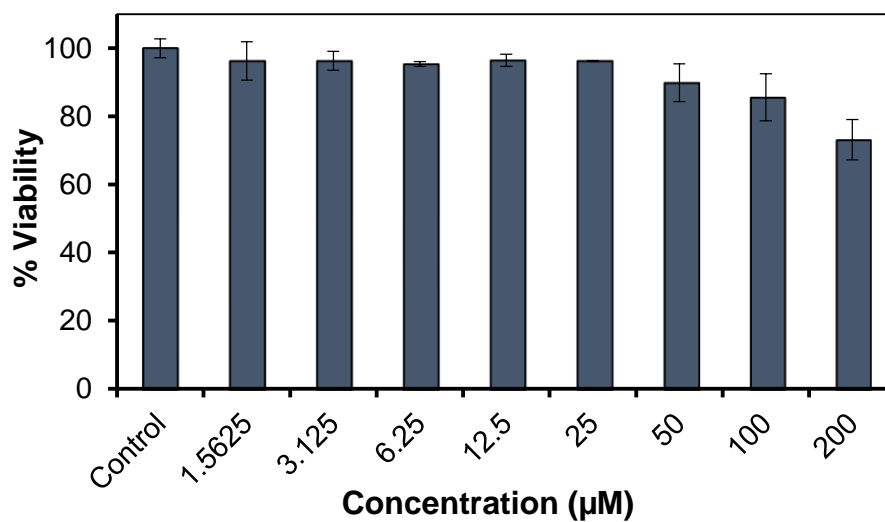3. J. Cui, G. Gao, H. Zhao, Y. Liu, H. Nie and X. Zhang, *New J. Chem.*, 2017, **41**, 11891–11897.

4. K. Tiensomjitr, R. Noorat, S. Chomngam, K. Wechakorn, S. Prabpai, P. Kanjanasirirat, Y. Pewkliang, S. Borwornpinyo and P. Kongsaeree, *Spectrochim. Acta Part A Mol. Biomol. Spectrosc.*, 2018, **195**, 136–141.

5. Y. Zhang, Y. Huang, Y. Yue, J. Chao, F. Huo and C. Yin, *Sensors Actuators, B Chem.*, 2018, **273**, 944–950.

6. S. Wang, S. Ma, J. Zhang, M. She, P. Liu, S. Zhang and J. Li, *Sensors Actuators, B Chem.*, 2018, **261**, 418–424.

7. Y. Jung, I. G. Ju, Y. H. Choe, Y. Kim, S. Park, Y.-M. Hyun, M. S. Oh, and D. Kim, *ACS Sens.* 2019, **4**, 441−449.

8. J, Xingzonga, L. Zhena, S. Mingqina, Y. Silib, Z. Xiaoyanga, Z. Yonglea, and H. Linxi, *Microchem. J.*, 2020, **152**, 104376.

9. C. Wu, R. Xie, X. Pang, Y. Li, Z. Zhou and H. Li, *Spectrochim. Acta Part A Mol. Biomol. Spectrosc.*, 2020, 118764.

10. Q. Jiang, Z. Wang, M. Li, J. Song, Y. Yang, X. Xu, H. Xu and S. Wang, *Tetrahedron Lett.*, 2020, **61**, 152103.

11. H. Yang, M. Li, Y. Zhang, S. Ruan, J. Yin, J. Song, Y. Yang, Z. Wang and S. Wang, *J. Lumin.*, 2020, **226**, 117436.

12. X. Li, J. Gu, H. Huang, Z. Zhou, J. Gao and Q. Wang, *Dye. Pigment.*, 2020, **181**, 108545.

13. J.-T. Hou, B. Wang, S. Wang, Y. Wu, Y.-X. Liao and W. X. Ren, *Dye. Pigment.*, 2020, **178**, 108366.

14. Z. Guo, Q. Niu, Q. Yang, T. Li, T. Wei, L. Yang, J. Chen and X. Qin, *Anal. Chim. Acta*, 2020, **1123**, 64–72.

15. B. B. Pavankumar, P. Ranjan, P. C. Jha and A. Sivaramakrishna, *Analyst*, 2020, **145**, 4615–4626.

16. X. Wang, G. Ding, Y. Wang, S. Mao, K. Wang and Z. Ge, Y. Zhang, X. Li, C.-H. Hung, *Tetrahedron*, 2020, **76**, 131726.

17. S. Mu, H. Gao, C. Li, S. Li, Y. Wang, Y. Zhang, C. Ma, H. Zhang and X. Liu, *Talanta*, 2021, **221**, 121606.

18. Q. Yi, J. He, X. Fu, J. Ying and L. Gong, J. Shen, and X. He, *Dye. Pigment.*, 2021, **196**, 109816.

19. A. Maiti, S. K. Manna, S. Halder, M. Mandal, A. Karak, D. Banik, K. Jana and A. K. Mahapatra, *Org. Biomol. Chem.,* 2022, **20**, 4949–4963.

20. Y. Z. Yang, M. Qing, X. Y. Luo, J. Xie and L. N. Zhang, *Spectrochim. Acta Part A Mol. Biomol. Spectrosc.*, 2022, **270**, 120795.

21. L. Liu, M. Xing, Y. Han, X. Zhang, P. Li, D. Cao, S. Zhao, L. Ma and Z. Liu, *Spectrochim. Acta Part A Mol. Biomol. Spectrosc.*, 2022, **264**, 120272.

22. N. Rao, Y. Le, D. Li, Y. Zhang, Q. Wang, L. Liu, and L. Yan, *Chem. Pap.*, 2022, **76**, 267–275.

23. D.-P. Li, L. Wei, X. Guo, X. Ran, T. Zhang, T. Zhang, H. Xiao and W. Shu, *RSC Adv.,* 2023, **13**, 35811–35815.

24. A. Maiti, D. Banik, S. Halder, S. K. Manna, A. Karak, K. Jana and A. K. Mahapatra, *Org. Biomol. Chem.*, 2023, **21**, 6046–6056.

25. C. O. Santos, S. T. A. Passos, J. E. P. Sorto, D. F. S. Machado, J. R. Correa, E. N. da Silva Júnior, M. O. Rodrigues and B. A. D. Neto, *Org. Biomol. Chem.*, 2023, **21**, 4606–4619.